Time-of-flight high-mass spectrometer observation of large size Nb clusters toward assembling of size controlled clusters

Takehiko Hihara[a] and Kenji Sumiyama
Institute for Materials Research, Tohoku University, Sendai 980-8577, Japan and CREST, Japan Science and Technology Corporation (JST), Japan

(Received 26 April 1999; accepted 9 July 1999)

Using a plasma-gas-condensation-type cluster source, we could obtain nano-scale clusters with the average diameter between 2 and 13 nm. In order to detect such large free clusters containing $1-10^5$ atoms, we have constructed a time-of-flight high-mass spectrometer (TOF-HMS). The size distribution of the Nb_n clusters observed by the TOF-HMS is in good agreement with the result of the transmission electron microscope observation. The mass spectra have been measured with varying the operational parameters of the cluster source. They are shifted to the smaller size direction and the mass distribution becomes narrower with increasing the He gas flow rate, V_{He}, and keeping the Ar gas flow rate, V_{Ar}, constant. These features are attributable to the decrease in the residence times of gaseous species in the cluster source. The cluster size increases with increasing the Ar gas pressure and lowering the temperature of the cluster source. © *1999 American Vacuum Society*. [S0734-211X(99)04005-6]

I. INTRODUCTION

There has been much interest in syntheses of nano-scale structure controlled materials such as nano-crystalline- and granular materials,[1–3] because their physical and chemical properties are different from those of uniform bulk materials.[4,5] Fabrication of these materials from nanometer sized clusters would be promising if we can produce and assemble the uniform size clusters.[6,7] As the first step, we have constructed a plasma-gas-condensation (PGC) cluster source, which is a combination of sputter vaporization and inert gas condensation techniques,[8–15] and successfully produced transition-metal clusters on substrates. Based upon the transmission electron microscope (TEM) observation, we have confirmed that the average cluster diameters, *d*, are between 2 and 13 nm. We have reported the unique electrical and magnetic properties of these monodispersed Co-cluster assemblies, i.e., the nonuniversal scaling behavior of the electrical conductivity in the two dimensional percolation process[16,17] and the marked temperature dependence of Coulomb-blockade-type tunnel conduction and magnetoresistance in CoO-coated Co cluster assemblies at low temperatures.[18]

If the small clusters migrate on the substrate and form larger islands, we cannot distinguish whether the nano-scale clusters are formed in the free space or on the substrate.[6,19] In this context, we wished to observe the sizes of nano-scale free clusters by mass spectrometry and compare the results with those of deposited clusters estimated by TEM observation. A time-of-flight mass spectrometer (TOF-MS) has been widely used to characterize a molecular beam and estimate the sizes of free clusters. The size dependent physical and chemical properties as well as their electronic states have been discussed with the results of the TOF-MS observation.[4,20] Since the above mentioned cluster size range (2–13 nm) in our PGC source corresponds to the number of atoms between 10^3 and 10^6, we have modified a standard Wiley–MacLaren-type[21] TOF to detect large clusters with the wide mass range of $1-10^7$ amu. The main difficulty in the TOF-MS detection of such large clusters flying from a cluster source is to adjust the drift distance in the flight tube because their initial velocities perpendicular to the TOF axis are usually very high. The possible solutions of this problem are as follows: (1) using special ion optics such as quadrupole focusing and reflecting optics after the acceleration plates,[22,23] (2) applying high potential at the acceleration plates to obtain the shorter flight time, (3) tilting the acceleration plates so as to compensate the initial velocity transverse to the flight path,[24] and (4) reduction of the flight tube length.

In the present Wiley–McLaren-type TOF high-mass spectrometer (TOF-HMS), the flight tube length was only 0.2 m, however, we obtained the mass resolution of the order of 1000. The cluster beam from the PGC source was collimated by slits with the gap of 2 mm corresponding to the ionization volume of 300 mm.[3] The large ionization volume was not necessary because a huge amount of clusters was already ionized in the cluster source by the Ar plasma in front of the sputtering target.[9] We simply used two rectangular multichannel plates (MCP) for the ion detection and a high electric potential for postacceleration to enhance the sensitivity of MCP in the high-mass range. In this article, we deal with the TOF-HMS spectra of Nb clusters produced by the PGC apparatus in comparison with the results of the TEM observation. We also describe the possibility of the cluster-size control using the results of the TOF-HMS spectra as functions of the operational parameters of the PGC cluster deposition system, i.e., He and Ar gas flow rates, their partial pressure in the growth chamber, and the temperature of the cluster source.

[a]Corresponding author; electronic mail: Hihara@imr.tohoku.ac.jp

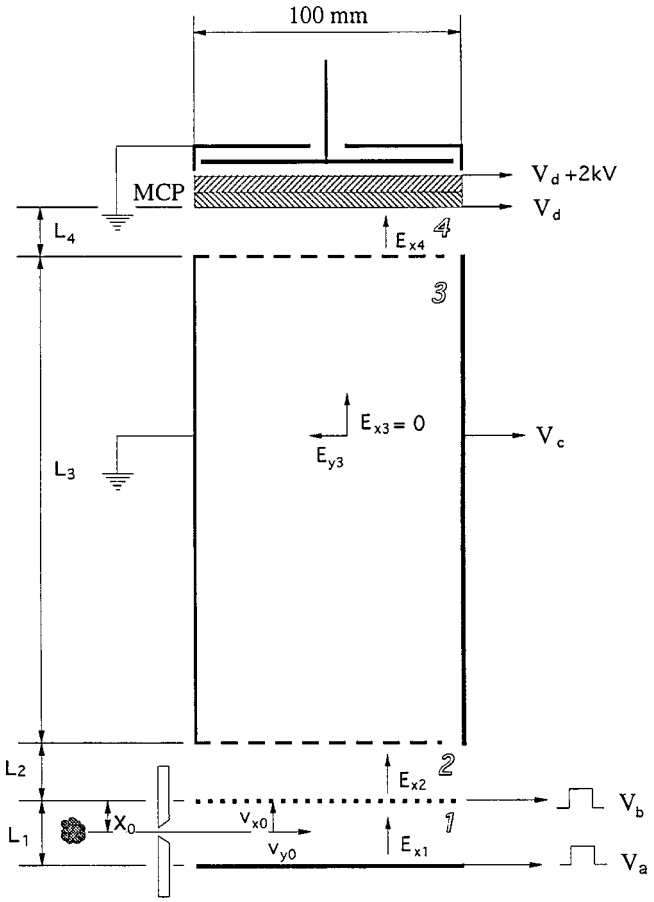

FIG. 1. Schematic diagram of the time-of-flight high-mass spectrometer. The ionized particles are collimated by the slits, entered into region 1, and accelerated by electric field $E_{x1}=(V_a-V_b)/L_1$. They are further accelerated by the electric field $E_{x2}=V_b/L_2$ and flight in region 3 of length L_3, where the electrostatic field, $E_{x3}=0$ (free-flight zone). In order to compensate for the initial velocity ν_{y0}, a perpendicular field $E_{y3}=V_c/0.1$ (V/m) can be applied. The ions are further postaccelerated by the electrostatic field of $E_{x4}=V_d/L_4$ and detected by multichannel plates (MCP).

II. DESIGN OF THE HIGH MASS SPECTROMETER

Figure 1 shows a schematic diagram of the spectrometer. A vacuum chamber (400×200×200 mm) for the TOF-HMS was evacuated down to 5×10^{-6} Pa by a turbo-molecular pump. The clusters enter in region 1 from the PGC cluster source through the collimators. The large fraction of clusters are already ionized in the cluster source via the Penning process.[9] They are extracted by the electric field of E_{x1} and further accelerated in region 2 by the electric field E_{x2}. The pulsed extraction potentials were generated by high voltage generators (Max-Electronics Co. Ltd., APL series) and high voltage push–pull switches (Behlke HTS 150-PGSM).[22] Region 3 is a field free zone where the clusters with the different mass-to-charge ratios are separated. In region 3, we can apply the electric field E_{y3} in order to steer the clusters along the perpendicular direction to the TOF axis. The incoming ionized clusters are postaccelerated by the electrostatic field E_{x4} in region 4 so as to increase the sensitivity of the MCP for large clusters. The signals were amplified by a preamplifier (EG&G Ortec VT-120C), sent to a discriminator (Fast Comtec 7011) and accumulated by a multichannel scaler (MCS) system (Fast Comtec 7885 MCD).

A. Acceleration of ions

A principle of the modified Wiley–McLaren-type TOF-MS has been already presented.[25,26] The cluster with a mass, m, and a charge, q, is collimated by the slits to determine the initial position x_0. In the following numerical expressions, we neglect the initial velocity component along the spectrometer axis, ν_{x0}. The total flight time, t, is then the sum of the four partial flight times, t_i, in each region i, and is given as follows:

$$t(X)=\sum_{i=1}^{4} t_i(X)=L_3\sqrt{\frac{m}{2qV_b}}\sum_{i=1}^{4} f_i(X), \tag{1}$$

where $X=x_0/L_3$ is the reduced initial position of the cluster and the other quantities in the equations are defined in Fig. 1. The term $f_i(X)$ is a dimensionless function expressed as follows:

$$\begin{aligned} f_1(X)&=2\sqrt{X/E},\\ f_2(X)&=2\frac{L_2}{L_3}(\sqrt{EX+1}-\sqrt{EX}),\\ f_3(X)&=1/\sqrt{EX+1},\\ f_4(X)&=\frac{2L_4}{\alpha L_3}(\sqrt{EX+1+\alpha}-\sqrt{EX+1}). \end{aligned} \tag{2}$$

Here, $E=\{(V_a-V_b)/L_1\}/(V_b/L_3)$ is the reduced electric fields in region 1 and $\alpha=V_d/V_b$ the reduced voltage in region 4. The sum of $f_i(X)$ with $i=1-4$, $f(X)$, is normally an order of 1.

Figure 2 shows $f(X)$ vs X with the different electric fields in region 1, E_{x1}. The mass resolution of the TOF system is described by

$$\frac{m}{\delta m}=\frac{1}{2}\frac{t}{\delta t}=\frac{1}{4}\frac{f(X_{\max})+f(X_{\min})}{f(X_{\max})-f(X_{\min})}, \tag{3}$$

which does not depend on mass and charge. The ionization volume is the restricted area between $X_{\min}$ and $X_{\max}$, where the mass resolution is independent of X. As shown in Fig. 2, the mass resolution decreases, while the ionization volume increases, as $X_{\max}-X_{\min}$ increases. An appropriate electric field, E_{x1}, should be applied in the region 1 in order to obtain a large ionization volume with a reasonable resolution.

For large cluster detection, the electric potential V_b in region 2 should be high enough to overcome the shift due to the initial velocity ν_{y0}. We also chose a rather short value of 0.2 m in L_3, and confined the large clusters within the detection area of the MCP during their total flight time. In order to obtain the plateau area between $X_{\max}$ and $X_{\min}$ in Fig. 2, the electric field, $E_{x1}=(V_a-V_b)/L_1$, is necessarily raised to around 138 kV/m, which corresponds to $V_a=10$ kV when $L_1=0.03$ m and $V_b=6$ kV. Nevertheless, we

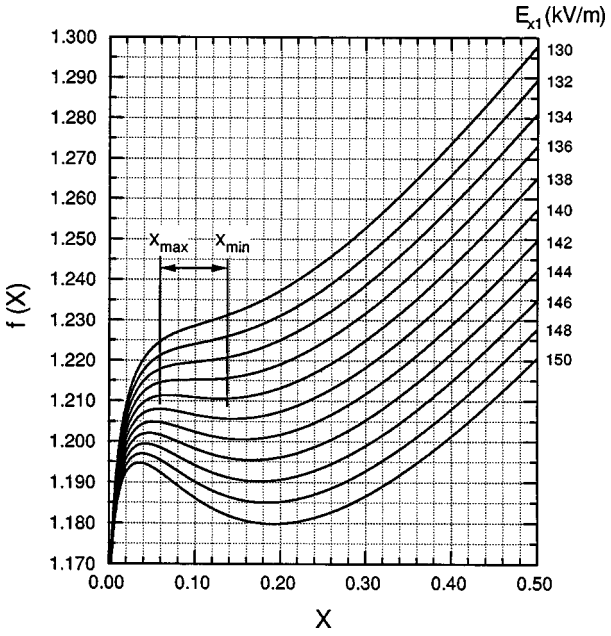

FIG. 2. Characteristic function of the TOF-HMS, $f(X)$, defined in Eqs. (1) and (2) vs the normalized initial position of the ionized clusters, X. It was calculated by Eq. (2) with $L_2=L_4=0.01$ m, $L_3=0.2$ m, $E_{x2}=600$ kV/m, and $E_{x4}=-700$ kV/m.

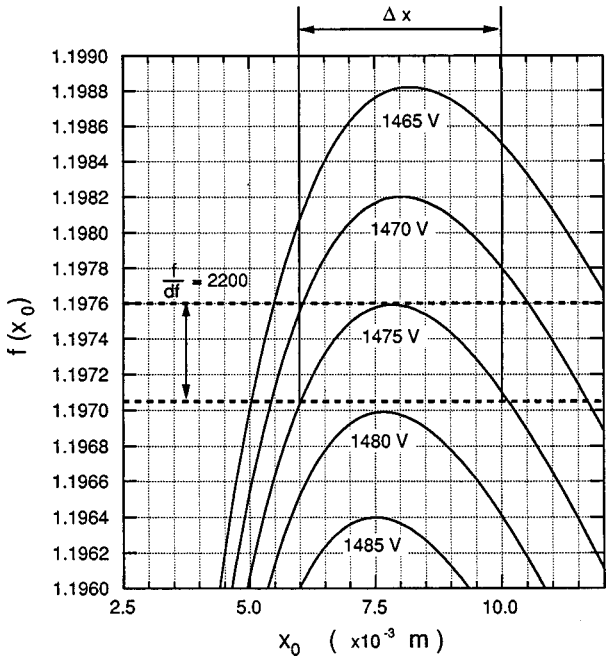

FIG. 3. Characteristic function of the TOF-HMS, $f(x_0)$, defined by Eqs. (1) and (2) as a function of x_0, instead of $X(=x_0/L_3)$, at the operating parameters. The cluster beam collimator is opened with the width $\Delta x=2$ mm. The parameters for the calculation are the same as in Fig. 2.

desired the potential voltage V_a to be less than 10 kV, because it was difficult for us to construct the high voltage circuit and switchers whose rise time is short enough. It should be noted that the rise time of the extraction voltage is a very important factor for the mass resolution. Therefore, we found optimum parameters so that $dt/dx=0$ within lower potential voltages. Figure 3 shows the $f(x_0)$ vs x_0 plots (instead of $X=x_0/L_3$) as a function of different V_a, with $L_1=L_2=L_4=0.01$ m, $L_3=0.2$ m, $V_a=7465-7485$ V, $V_b=6$ kV and $V_d=-7$ kV. The optimized electric potential V_a is found to be 7475 V with the reasonable resolution $f/\delta f=2200\,(m/\delta m=1100)$ and $\Delta x=2$ mm corresponding to the ionization volume of 300 mm^2.

B. Ion steering optics

Since the clusters from the PGC source have a translational velocity along the beam axis, ν_{y0}, they move to the perpendicular direction to the TOF axis during the total flight time, t. Therefore, when the clusters are too heavy, they will stray off the effective detection area of the MCP. In our TOF system, the deflection electric field, $E_{y3}=V_c/0.1$ (V/m), can be applied through the wide deflection plate for steering the heavy clusters. The total drift length of the cluster, $Y_{\mathrm{MCP}}(m,E_{y3})$, along the perpendicular direction to the TOF axis after the time of flight t can be given by the following equation:

$$Y_{\mathrm{MCP}}(m,E_{y3})=\nu_{y0}t-\frac{q}{2m}E_{y3}t_3^2-\frac{q}{m}E_{y3}t_4t_3. \tag{4}$$

Figure 4 shows the calculated Y_{MCP} for the different E_{y3} values. Here, the initial velocity ν_{y0} is assumed to be independent of the cluster size and to be approximately 300 m/s, which is close to that of the carrier Ar gas.[23] In order to increase the mass range of the TOF system, a wide detection area was desired. We used 100×15 mm MCP so as to detect the clusters with the mass of $1-5\times10^6$ amu at $V_c=0-3$ kV.

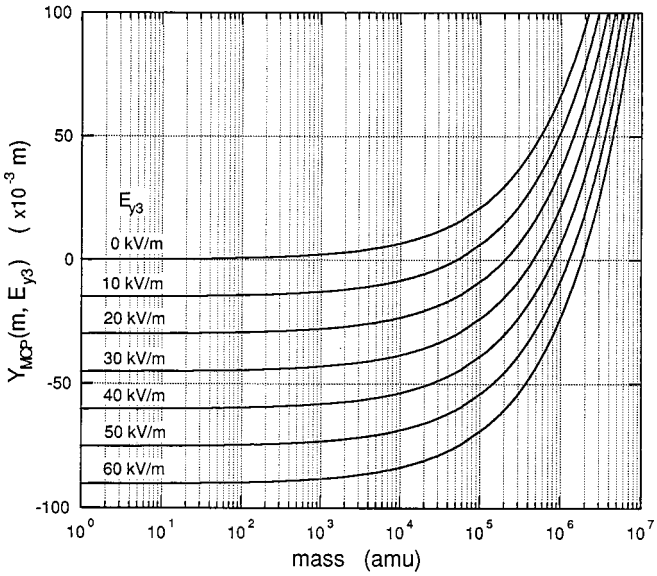

FIG. 4. Deflection length of the clusters by the electrostatic field of E_{y3}, so as to compensate for the initial velocity ν_{y0} perpendicular to the TOF axis. The ν_{y0} value is assumed to be 300 m/s.

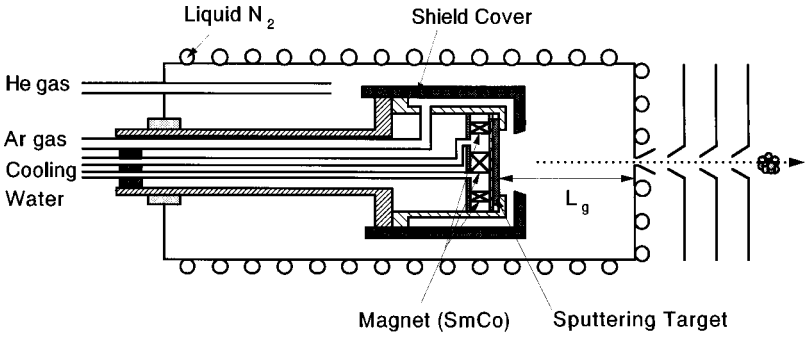

FIG. 5. Schematic diagram of plasma-gas-condensation (PGC)-type cluster source. Ar gas is introduced in the sputtering source through the small gap between target and shield cover. He gas is injected from the backside of the cluster source.

C. Detector

The ion detector consists of two MCP in series. The incoming ions were postaccelerated by a high voltage V_d of -7 kV before reaching the MCP. Across each MCP, 1 kV potential was applied. The electrons emitted from the rear MCP were accelerated by an additional 5 kV potential onto a collector plate, producing a pulse current, which was sent to the data acquisition electronics as a count.

The signal intensity of the MCP depends on the incident velocity of the cluster. It decreases with increasing the cluster mass, because the total kinetic energy of the cluster obtained from the electric fields is independent of their mass. Consequently, the sensitivity of the MCP decreases with increasing the cluster mass. It has been reported that the threshold is about 1.5×10^6 amu for Cs clusters and 1.5×10^5 amu for Li clusters when the postacceleration voltage is 8 kV.[23] In our experimental setup, the total acceleration potential is higher than 13 kV, which would be sufficient to detect the large clusters generated by the present PGC cluster source. To confirm this, we compared the cluster size detected by our TOF-HMS with that by TEM observation as we will describe in Sec. IV.

III. EXPERIMENT

Nb clusters were synthesized by a PGC apparatus, whose details have been described elsewhere.[15] In this work, we changed the sputtering source as shown in Fig. 5. A continuous Ar gas stream was injected through the 0.3 mm gap between the shield cover and the target in order to avoid the accumulation of formed particles which induce the abnormal discharge and the short circuit during the glow discharge operation.[10] The metal vapors were generated from a Nb target by dc magnetron sputtering. Clusters nucleate in a high pressure Ar gas atmosphere (0.2–0.7 kPa) and grow in the space between the target and the nozzle (the growth region), whose length, L_g, can be varied by moving the sputtering source back and forth. He gas was also introduced into the sputtering chamber from the backside of the source. The cluster beam was extracted through the nozzle of 5 mm in diameter by differential pumping and further collimated by the three skimmers.

For a TEM observation, a microgrid, which is a carbon-coated colodion film supported by a Cu grid, was used as a substrate. The deposition rate was measured by a quartz thickness monitor. The samples were exposed in air for transportation and observed with an Hitachi HF-2000 electron microscope, operating at 200 kV. The TEM images were taken as digitized data with a slow-scan charge coupled device (CCD) camera installed in the electron microscope.

IV. RESULTS

Figure 6(a) shows a typical bright-field TEM image of the Nb clusters prepared at $L_g=200$ mm, $V_{\mathrm{Ar}}=V_{\mathrm{He}}=3.0\times10^{-4}$ mol/s (400 sccm), $p_s=380$ Pa, and $P_W=300$ W. Here, V_{Ar} and V_{He} are the flow rate of Ar and He gases, respectively, p_s the total pressure in the cluster source, and

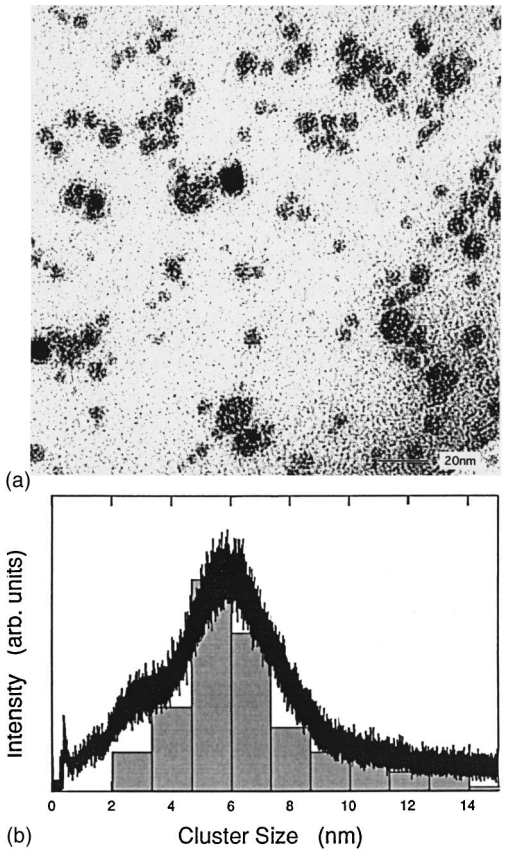

FIG. 6. (a) TEM image of the nanometer size Nb clusters observed by TEM obtained with $V_{\mathrm{Ar}}=V_{\mathrm{He}}=3.0\times10^{-4}$ (400 sccm), $p_s=380$ Pa, and $P_W=300$ W. (b) The histogram of cluster size distribution estimated from the TEM image in (a) and the notched line from the TOF spectrum.

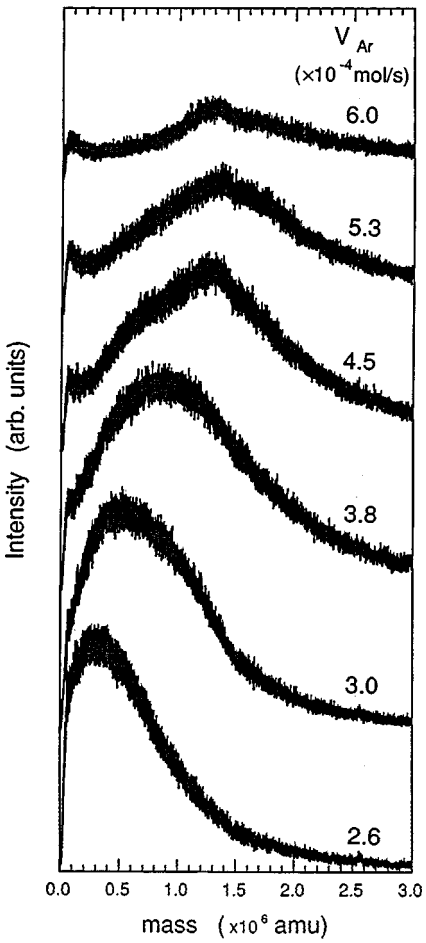

FIG. 7. Mass spectra of Nb clusters prepared with $P_W=300$ W, $V_{Ar}=2.6-6.0\times10^{-4}$ (350–800 sccm), and the constant V_{He} of 3.0×10^{-4} mol/s (400 sccm).

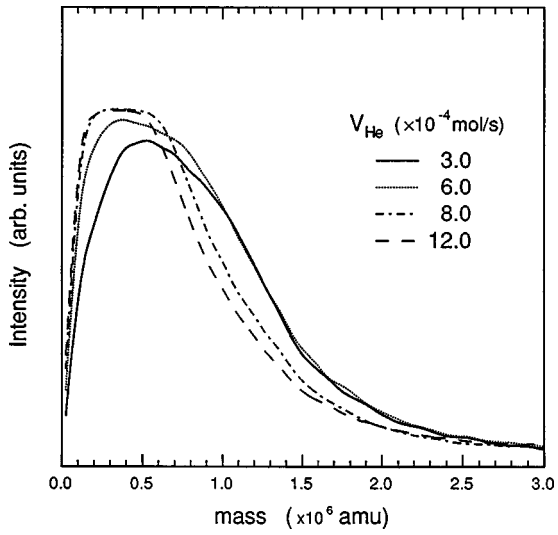

FIG. 8. Mass spectra of Nb clusters prepared with $P_W=300$ W, $V_{Ar}=3.0\times10^{-4}$ (400 sccm), and $V_{He}=3.0-12\times10^{-4}$ mol/s (400–1600 sccm).

P_W the sputtering power. The corresponding size distribution histogram estimated from the deposited area of 0.036 μm^2 is shown in Fig. 6(b). The clusters are dispersed in the size range of between 2 and 15 nm. The mean size of the Nb clusters is about 7 nm. The TOF spectrum of the Nb clusters as a function of diameter is also indicated in Fig. 6(b). Here, we converted the mass of the Nb cluster into its diameter by assuming the bulk Nb density. Both are well overlapped within the observed size range above 2 nm in diameter.

Figure 7 shows the TOF spectra sequence of the Nb clusters operated at $L_g=200$ mm, $P_W=300$ W, $V_{Ar}=2.6-6.0\times10^{-4}$ mol/s (350–800 sccm), $p_s=350-620$ Pa, and the constant V_{He} of 3.0×10^{-4} mol/s (400 sccm). The spectrum at $V_{Ar}=2.6\times10^{-4}$ mol/s (350 sccm) exhibits a broad distribution with the maximum at 0.4×10^6 amu. The peak in the mass spectrum shifts toward the higher mass direction with increasing V_{Ar} up to 5.3×10^{-4} mol/s. The mass spectrum becomes broader and its intensity decreases with increasing V_{Ar}. With further increasing V_{Ar} above 5.3×10^{-4} mol/s, the mean cluster size slightly decreases. One can also see the small peak at around 1×10^5 amu for $V_{Ar}\geq4.5\times10^{-4}$ mol/s. These results indicate that the Ar gas pressure influences not only the nucleation and growth of the clusters but also the sputtering yield.

Figure 8 shows the TOF spectra sequence of the Nb clusters synthesized at $L_g=200$ mm, $P_W=300$ W, $V_{Ar}=3.0\times10^{-4}$ mol/s (400 sccm) and $V_{He}=3.0-12\times10^{-4}$ mol/s (400–1600 sccm), $p_s=380-650$ Pa. These spectra were mathematically smoothed to emphasize the spectral differences. The mean cluster size becomes small with increasing V_{He}, although the total inert-gas pressure in the cluster source increases. This result is contradictory to the variation of the mass spectra taken with changing V_{Ar}. It is also seen that the mass spectrum becomes narrow when increasing V_{He} with the constant V_{Ar}. These results suggest that the He gas reduces the residence time of the gaseous species inside of the cluster source, as we will discuss in Sec. V.

In order to investigate the temperature effect on the cluster size, we cooled the PGC cluster source by liquid N_2. Figure 9 shows the TOF spectra sequence of the Nb clusters obtained at the different sputtering power, $P_W=200-350$ W, $L_g=200$ mm, and $V_{Ar}=V_{He}=3.0\times10^{-4}$ mol/s (400 sccm). The clusters become slightly larger with increasing P_W, owing to the increase in the density of the vaporized atoms. When the cluster source and the nozzle are cooled by liquid N_2, the mass distribution of the clusters shifts toward the larger size direction and becomes broader, suggesting that the residence time of the gaseous species is increased by cooling (see Sec. V).

V. DISCUSSION

The observation of the cluster size by the TOF-MS is sometimes misleading. The detection probability of the MCP is strongly mass dependent.[23] It is also possible that the doubly ionized clusters are produced in the PGC cluster source, which have shorter flight time in the TOF-MS. The cluster size estimated from the TEM photograph is, however, con-

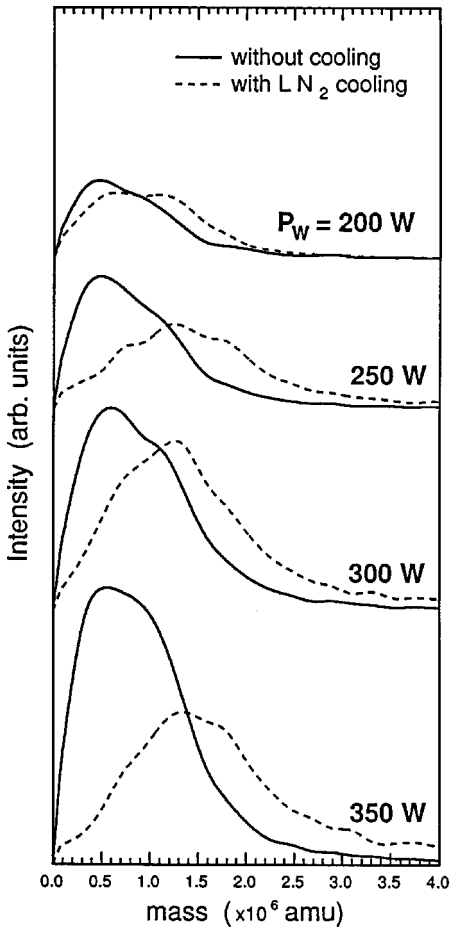

FIG. 9. Mass spectra of Nb clusters prepared with $P_W = 200-350$ W and $V_{Ar} = V_{He}\, 3.0\times10^{-4}$ (400 sccm).

sistent with the mass distribution measured with our TOF-HMS in the size range between 2 and 15 nm except for the smaller clusters. In the bright-field imaging mode, such small clusters can hardly be distinguished from the background image of the amorphous carbon film. This is particularly true for the clusters whose orientation is not strongly diffracting with respect to the incident electron beam direction. Another problem is that the atoms and the smaller clusters can move on the substrate and coalesce to form larger clusters.[6,19,27] This effect will be observed when a large amount of atoms and smaller clusters ($d<1$ nm) are produced in the cluster source. However, we have not found any clear evidence for the surface migration within the present operation parameters.

The cluster size can be controlled in the PGC method.[13,15] The important experimental parameters are the sorts of the inert gas, i.e., He and/or Ar, their partial pressure (the mixing ratio) in the cluster source and the sputtering power. According to the inert gas condensation process, the metal vapor is cooled by collisions with the cold inert gas atoms. In general, since the thermal energy transfer from the metal vapor during the collision process is much more effective for heavier inert gases, the atomic vapor condensation is promoted more effectively in the Ar gas than in the He gas: the larger clusters are formed in the heavier inert gas.[28] This explanation can be reasonable but not enough to understand the present experimental results, because the smaller clusters with narrower size distribution were obtained when the total pressure in the cluster source was increased by introducing more He gas with the constant V_{Ar} (see Fig. 8).

In an isentropic flow of compressible fluids, a critical pressure p^* can be defined as[29,30]

$$p^* = p_s\{2/(\gamma+1)\}^{\gamma/(\gamma-1)}, \tag{5}$$

where p_s is the pressure in the cluster source and $\gamma=5/3$ the ratio of molar heat capacity for the monatomic He and Ar gases. Within our experimental condition, the back pressure after the exit nozzle was much lower than p^*. In this case, the mass flow rate, $\dot{m}$, through the nozzle can be formulated by the following equation within the standard gas dynamics:[30]

$$\dot{m} = \frac{A_n p_s}{\sqrt{k_B T_s}} \sqrt{\gamma m \left(\frac{2}{\gamma+1}\right)^{(\gamma+1)/(\gamma-1)}}, \tag{6}$$

where k_B is the Boltzmann constant, T_s the gas temperature in the cluster source, A_n the cross section of the nozzle, and m the atomic mass of the inert gas. In the present experimental setup, the total amount of the incoming inert gases was estimated by the mass flow meter (V_{Ar} and V_{He}). The estimated $\dot{m}$ values from Eq. (6) were roughly in agreement with the sum of V_{Ar} and V_{He}. This fact suggests that the gas dynamics through the nozzle is isentropic and Eq. (6) is fulfilled at the exit nozzle. The drift velocity of the gaseous species in the cluster source, ν_z, can then be estimated by the following equation (the perfect gas equation):

$$\nu_z = \frac{\dot{m} k_B T_s}{m A_s p_s}, \tag{7}$$

where A_s is the cross section of the cluster source (1.4×10^{-2} m^2). Combining Eqs. (6) with (7), we can express the residence time of the gaseous species in the cluster source as follows:

$$t_s = L_g \nu_z^{-1} = L_g \frac{A_s}{A_n} \sqrt{\frac{m}{\gamma k_B T_s} \left(\frac{\gamma+1}{2}\right)^{(\gamma+1)/(\gamma-1)}}. \tag{8}$$

When p_s increases, the gases are more compressed at the nozzle and the flow rate of the exit gases increases. Accordingly, t_s becomes independent of p_s for the isentropic flow.

In the present experimental results, the important parameters to determine the cluster size are the residence time, t_s, and the gas pressure, p_s, in the cluster source. Based upon the cluster growth model by the inert gas condensation,[15] the smaller cluster can be obtained when the residence time becomes shorter, because the total number of cluster–cluster and/or cluster-vapor atom collisions can be proportional to t_s. The t_s value decreases when the He gas is introduced into the cluster source, because the mass and viscosity of He atom are one order smaller than those of Ar, and He gas is more effectively ejected than Ar gas. The nozzle temperature also influences the cluster size. According to Eq. (8), the residence time increases with decreasing T_s: the gaseous

species flow more slowly in the cluster source. Therefore, as shown in Figs. 8 and 9, the peak in the mass spectra shifts toward the lower mass side with increasing V_{He} and T_s.

When the sputtering power is increased, the clusters become slightly larger (see Fig. 9). In the first stage of the cluster formation, the atomic vapor condensation is thought to be the dominant process for promoting the cluster growth, where the collision frequency between the vaporized atoms affects the cluster size. With increasing P_W, the density of the vaporized atoms from the sputtering target increases, so that the clusters become larger in such stochastic process. Moreover, when the mixing ratio of the He and Ar gases is not changed and t_s is constant, the gas pressure in the cluster source, p_s, can be also an indicative parameter for the cluster size. As shown in Fig. 7, the mean cluster size increases when increasing V_{Ar} (and p_s). This result indicates that the nucleation and growth are promoted by the Ar gas pressure, because the collision frequency among the vaporized atoms and the inert gas increases proportionally to p_s. On the other hand, the sputtering yield is affected not only by the sputtering power P_W but also by p_s. It has been reported that the sputtering yield is suppressed with increasing p_s.[8] This trend can be interpreted as a result of the decrease of the mean free path of the Ar gas: the incident energy of the Ar ions into the target decreases and/or the amount of vaporized atoms returning to the target increases with increasing p_s. We have not clearly observed this effect up to $V_{Ar}=5.3\times10^{-4}$ mol/s, whereas the peak in the mass spectrum slightly shifts to the lower mass side when V_{Ar} increases from 5.3×10^{-4} to 6.0×10^{-4} mol/s.

VI. CONCLUSION

We have constructed a time-of-flight high-mass spectrometer (TOF-HMS) attached to the plasma-gas-condensation (PGC)-type cluster source. Large clusters consisting of more than 3 million atoms (about 15 nm in diameter) were detected by the TOF-HMS. The size distribution of the large Nb clusters estimated from TEM image was in good agreement with the mass spectrum.

The present TOF-HMS study with varying the source parameters demonstrates that the cluster size is reduced and the size dispersion is narrowed by the He gas flow. The temperature of the cluster source also affects the cluster size: larger clusters are formed by cooling the cluster source. The Ar gas pressure influences not only the cooling efficiency for the metal atoms but also the sputtering yield. Increasing the Ar flow rate, V_{Ar}, the cluster nucleation and growth are promoted, leading to formation of larger clusters, while, the sputtered vapor density decreases, when we increase the V_{Ar} value over 5.3×10^{-4} mol/s.

ACKNOWLEDGMENTS

The authors wish to thank Dr. T. J. Konno for support to the TEM observation, Dr. M. Sakurai for helpful suggestions, and Dr. S. Yamamuro for useful comments. The authors gratefully acknowledge technical contributions to the PGC cluster deposition apparatus and the TOF-HMS from Vieetech Japan Co., Ltd. This work was supported by CREST (Core Research for Evolutional Science and Technology) of Japan Science and Technology Corporation (JST). The authors are also indebted to the Laboratory for Developmental Research of Advanced Materials, Institute for Materials Research, Tohoku University.

[1] A. S. Edelstein and R. C. Cammarata, in *Nanomaterials: Synthesis, Properties and Applications* (Institute of Physics, Bristol, 1996).
[2] B. Barbara, J. Magn. Magn. Mater. **156**, 123 (1996).
[3] P. Melinon, V. Paillard, V. Dupuis, A. Perez, P. Jensen, A. Hoareau, J. P. Perez, J. Tuaillon, M. Broyer, J. L. Vialle, M. Pellarin, B. Baguenard, and J. Lerme, Int. J. Mod. Phys. B **9**, 339 (1995).
[4] W. A. deHeer, Rev. Mod. Phys. **65**, 611 (1993).
[5] H. Haberland, in *Clusters of Atoms and Molecules I and II* (Springer, Berlin, 1995).
[6] K. Bromann, C. Félix, H. Brune, W. Harbich, R. Monot, J. Buttet, and K. Kern, Science **274**, 956 (1996).
[7] M. Ehbrecht, B. Kohn, F. Huisken, M. A. Laguna, and V. Paillard, Phys. Rev. B **56**, 6958 (1997).
[8] S. Yatsuya, T. Kamakura, K. Yamauchi, and K. Mihama, Jpn. J. Appl. Phys., Part 2 **25**, L42 (1986).
[9] H. Haberland, M. Karrais, M. Mall, and Y. Thurner, J. Vac. Sci. Technol. A **10**, 3266 (1992).
[10] H. Haberland, M. Mall, M. Moseler, Y. Qiang, T. Reiners, and Y. Thurner, J. Vac. Sci. Technol. A **12**, 2925 (1994).
[11] M. Goto, J. Murakami, Y. Tai, K. Igarashi, and S. Tanemura, Z. Phys. D **40**, 115 (1997).
[12] G. Hohl, T. Hihara, M. Sakurai, T. Oishi, K. Wakoh, K. Sumiyama, and K. Suzuki, Jpn. J. Appl. Phys., Part 1 **33**, 1509 (1994).
[13] S. Yamamuro, M. Sakurai, T. J. Konno, K. Sumiyama, and K. Suzuki, AIP Conf. Proc. **416**, 491 (1997); S. Yamamuro, K. Sumiyama, M. Sakurai, and K. Suzuki, Supramol. Sci. **5**, 239 (1998).
[14] S. Yamamuro, K. Sumiyama, and K. Suzuki, J. Appl. Phys. **85**, 483 (1999).
[15] T. Hihara and K. Sumiyama, J. Appl. Phys. **84**, 5270 (1998).
[16] S. Yamamuro, K. Sumiyama, T. Hihara, and K. Suzuki, J. Phys. Soc. Jpn. **68**, 28 (1999).
[17] S. Yamamuro, K. Sumiyama, T. Hihara, and K. Suzuki, J. Phys.: Condens. Matter **11**, 3247 (1999).
[18] D. L. Peng, K. Sumiyama, S. Yamamuro, T. Hihara, and T. J. Konno, Appl. Phys. Lett. **74**, 76 (1999).
[19] G. M. Francis, L. Kuipers, J. R. A. Cleaver, and R. E. Palmer, J. Appl. Phys. **79**, 2942 (1996).
[20] J. P. Bucher and J. A. Bloomfield, Int. J. Mod. Phys. B **7**, 1079 (1993).
[21] W. C. Wiley and I. H. McLaren, Rev. Sci. Instrum. **26**, 1150 (1955).
[22] T. Bergmann, H. Goehlich, T. P. Martin, H. Schaber, and G. Malegiannakis, Rev. Sci. Instrum. **61**, 2585 (1990).
[23] U. Zimmermann, N. Malinowski, U. Näher, S. Frank, and T. P. Martin, Z. Phys. D **31**, 85 (1994).
[24] C. W. S. Conover, Y. J. Twu, Y. A. Yang, and L. A. Bloomfield, Rev. Sci. Instrum. **60**, 1065 (1989).
[25] F. Chandezon, B. Huber, and C. Ristori, Rev. Sci. Instrum. **65**, 3344 (1994).
[26] P. Piseri, S. Iannotta, and P. Milani, Int. J. Mass Spectrom. Ion Processes **153**, 23 (1996).
[27] C. Félix, G. Vandoni, W. Harbich, J. Buttet, and R. Monot, Surf. Sci. **331–333**, 925 (1995).
[28] P. Pfau, K. Sattler, J. Mühlbach, R. Pflaum, and E. Recknagel, J. Phys. F **12**, 2131 (1982).
[29] O. F. Hagena, Surf. Sci. **106**, 101 (1981).
[30] D. R. Miller, in *Atomic and Molecular Beam Methods*, edited by G. Scoles (Oxford University Press, Oxford, 1988), Vol. 1.